Fatigue crack propagation in short-fiber reinforced plastics

K. Tanaka
Department of Mechanical Engineering, Meijo University, Nagoya 468-8502, Japan
ktanaka@meijo-u.ac.jp

K. Oharada, D. Yamada
Graduate School, Meijo University, Nagoya 468-8502, Japan

K. Shimizu
Department of Mechanical Engineering, Meijo University, Nagoya 468-8502, Japan

ABSTRACT. The influence of fiber orientation on the crack propagation behavior was studied with single edge-notched specimens which were cut from an injection-molded plate of short-fiber reinforced plastics of polyphenylenesulphide (PPS) reinforced with 30wt% carbon fibers. Specimens were cut at five fiber angles relative to the molding direction, i.e. $\theta = 0°$ (MD), 22.5°, 45°, 67.5°, 90° (TD). Fracture mechanics parameters derived based on anisotropic elasticity were used as a crack driving force. Macroscopic crack propagation path was nearly perpendicular to the loading axis for the cases of MD and TD. For the other fiber angles, the crack path was inclined because the crack tended to propagate along inclined fibers. For mode I crack propagation in MD and TD, the resistance to crack propagation is improved by fiber reinforcement, when the rate is correlated to the range of stress intensity factor. The crack propagation rate, da/dN, was slowest for MD and fastest for TD. For each material, the crack propagation rate is higher for larger R ratio. The effect of R ratio on da/dN diminished in the relation between da/dN and the range of energy release rate, ΔG_I. Difference among MD, TD and matrix resin becomes small when da/dN correlated to a parameter corresponding the crack-tip radius, $H\Delta G_I$, where H is compliance parameter. Fatigue cracks propagated under mixed loading of mode I and II for the fiber angles other than 0° and 90°. The data of the crack propagation rate correlated to the range of total energy release rate, ΔG_{total}, lie between the relations obtained for MD and TD. All data of crack propagation tend to merge a single relation when the rate is correlated to the range of total energy release rate divided by Young's modulus.

KEYWORDS. Fatigue crack propagation; Short-fiber reinforced plastics; Fiber orientation; Fracture mechanics.

INTRODUCTION

S hort-fiber reinforced plastics (SFRP) are expected to be used more widely in order to reduce the weight of vehicles such as automobiles, because the injection molding process makes high-rate and economical production possible. Their application in fatigue-sensitive components has steadily increased in automobile industries. Under cyclic loading, fatigue cracks are formed relatively early in machine components and the propagation process occupies the most part of the fatigue life. The propagation behavior of fatigue cracks is highly anisotropic, depending on the fiber orientation

[1-5]. The path of crack propagation is influenced by the fiber orientation even if the applied load is uniaxial, and cracks often propagate under mixed mode condition. In most of the previous works, the fatigue crack propagation rate has been correlated to the stress intensity factor or the energy release rate which are derived based on isotropic elasticity even though SFRP are anisotropic.

In the present paper, the crack propagation behavior was studied with polyphenylenesulphide (PPS) reinforced with 30wt% carbon fibers. Specimens with single edge notch were cut at different orientation angles with respect to the molding flow direction from plates made by injection molding. Fatigue crack propagation tests were conducted at stress ratios of 0.1 and 0.5. The influences of fiber orientation on the crack path and the crack propagation rate was studied from a viewpoint of fracture mechanics based of anisotropic elasticity.

EXPERIMENTAL PROCEDURE

Specimens

The materials is short-fiber reinforced brittle thermoplastics, polyphenylene sulphite (PPS), reinforced with carbon fibers. The amount of fiber content was 20 wt%. Fatigue specimens were cut from an injection-molded plate (IMP) with the in-plane dimensions of 80×80 mm and the thickness of 1 mm. Fig. 1 shows the shape of test specimens which has a single edge notch of length 2 mm, the length of 80mm, and the width of 20mm. The region of length 15mm was used for chucking to the testing machines through aluminium tabs. A fatigue crack was started from the initial notch. The angle between molding direction and longitudinal direction of specimens was set to be five values: $\theta =$ 0° (MD), 22.5°, 45°, 67.5°, 90° (TD). Since the fiber direction on the skin layer of injection-molded plates is nearly along the molding flow direction (MFD), the angle θ means the angle between the fiber direction and the loading axis. In the following, the angle θ is called the fiber angle. Injection-molded plates have a three-layer structure where two skin layers sandwich the core layer [5]. The thickness of the core layer of the present plates was about 0.15 mm. Experimentally measured values of anisotropic elastic constants of IMP are summarized in Tab. 1. Young's modulus for various fiber angles are given in Tab. 2. Specimens made of only the matrix resin PPS were also made from the injection-molded plate with thickness 1mm. They are isotropic having Young's modulus of 4.45GPa, and Poisson's ratio of 0.368.
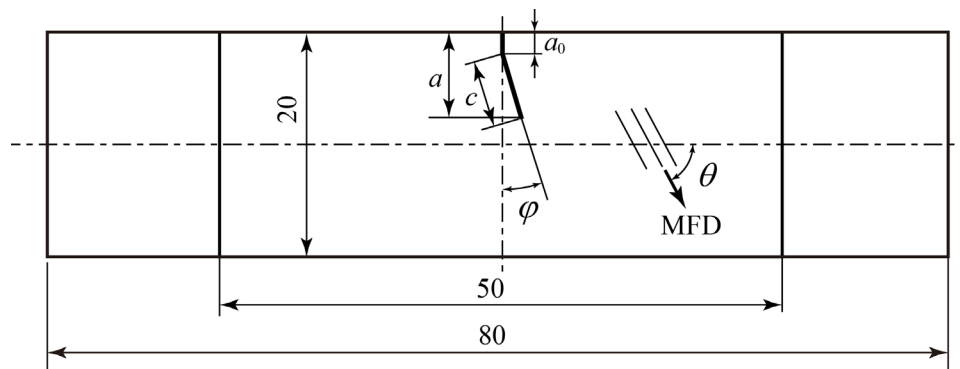

Figure 1: Single edge notched plate.

E_1 (GPa)	ν_{12}	E_2 (GPa)	(ν_{21})	G_{12} (GPa)
22.78	0.378	10.84	(0.177)	4.86

Table 1: Elastic constants of IMP.

Fiber angle	0° (MD)	22.5°	45°	67.5°	90°(TD)	Matrix
Young's modulus E (GPa)	22.8	18	12.9	11.1	10.8	4.45

Table 2: Young's modulus for various fiber angles.

Fatigue Crack Propagation Tests

Fatigue tests were performed with a tension-compression electro-servo-hydraulic testing machine. Fatigue testing was done in air at room temperature under load-controlled conditions with the load ratio *R* of 0.1 and 0.5. The waveform of the cyclic load was triangular and the frequency was between 2.5 and 8 Hz. The crack length was measured with a video microscope at the magnification of 100. Fig. 1 illustrates a fatigue crack formed from the notch. The angle of the macroscopic direction of crack propagation, φ, and the crack length, *c*, were measured experimentally. The crack length projected on the plane perpendicular to the loading axis is denoted by *a* as shown in Fig. 1. The crack propagation rate is calculated from the crack length along crack propagation direction.

Fracture Mechanics Parameters

The macroscopic crack path was perpendicular to the loading axis for the cases of $\theta = 0°$ (MD) and 90° (TD), while inclined for the other fiber angles. Using the macroscopic crack angle measured experimentally, the energy release rate of crack propagation was calculated by the method of a modified crack closure integral of the finite element method (FEM) [6]. The details of FEM are described in Appendix.

The energy release rate of is expressed as

$$G_{\mathrm{I}} = \sigma^2 \pi a \cdot Y_{\mathrm{I}}\left(a/W\right), \quad G_{\mathrm{II}} = \sigma^2 \pi a \cdot Y_{\mathrm{II}}\left(a/W\right) \tag{1}$$

where σ is the applied gross stress, *a* is crack length, *W* is plate width, $Y_{\mathrm{I}}(a/W)$ and $Y_{\mathrm{II}}(a/W)$ are correction coefficients for mode I and II loading. For the case of collinear crack growth for MD and TD specimens, the energy release rate is converted to the stress intensity factor by using [7]

$$G_{\mathrm{I}} = H_{\mathrm{I}} K_{\mathrm{I}}^2, \quad \text{where} \quad H_{\mathrm{I}} = \sqrt{\frac{1}{2E_1 E_2}} \left[\sqrt{\frac{E_1}{E_2}} + \frac{-2\left(\nu_{12}/E_1\right) + \left(1/G_{12}\right)}{2\left(1/E_1\right)} \right]^{1/2} \tag{2}$$

The $1/H_{\mathrm{I}}$ value for MD is 17.4 GPa, and 12.0 GPa for TD. For isotropic materials, we have $G_{\mathrm{I}} = K_{\mathrm{I}}^2/E$. For MD and TD, G_{I} can be converted to the stress intensity factor, K_{I}, by the above equation. The value of K_{I} is expressed as

$$K_{\mathrm{I}} = \sigma\sqrt{\pi a} \cdot F_{\mathrm{I}}\left(a/W\right) \tag{3}$$

where $F_{\mathrm{I}}(a/W)$ is a correction factor.

EXPERIMENTAL RESULTS AND DISCUSSION

Fatigue Crack Propagation Path

Optical micrographs of cracks for MD, 45°, and TD specimens fatigued under $R = 0.1$ are shown in Fig. 2, respectively, where the square region shown in (a), (c),(e) are enlarged in (b), (d), (f). For MD and TD specimens, the crack path is microscopically zigzag shaped and macroscopically straight perpendicular to the loading direction. On the other hands, the crack path of 45° specimen is inclined, making the angle of $\varphi = 24.4°$ with respect to the plane perpendicular to the loading axis. The microscopic crack path is either in the matrix or along fibers. For MD specimens, the crack propagation is blocked by fibers and circumvents fibers along fiber surfaces, showing zigzag path. For TD specimens, the crack path is less tortuous following the fiber direction. For 45° specimens, the crack propagates nearly 45° along the fiber and turns to horizontal in the matrix. The macroscopic direction is a combination of these two paths and is less than the fiber angle of 45°.

The macroscopic crack path for 22.5° and 67.5° specimens was not perpendicular to the loading axis. Fig. 3 shows the change of crack propagation angle φ with the fiber angle θ for $R = 0.1$ and 0.5. The dotted line in the figure indicates the

crack path is coincident to the fiber angle, i.e. $\varphi = 90 - \theta$ (deg). There is no big difference between $R = 0.1$ and 0.5. The crack angle increases with decreasing fiber angle, and takes a maximum at 22.5°. The crack angle for the cases of $\theta = 22.5°, 45°, 67.5°$ is below the dotted line, because the macroscopic crack path consists of the matrix path with $\varphi \approx 0$ and fiber path with $\varphi \approx 90 - \theta$.

Fatigue Crack Propagation under Mode I Loading
The fatigue crack propagation rate for MD and TD specimens is plotted against the range of stress intensity factor, ΔK, in Fig. 4(a). Both for $R=0.1$ and 0.5, the crack propagation rate is lower in MD than in TD. The resistance to crack propagation is improved by fiber reinforcement, and fibers aligned perpendicular to the crack growth direction block more severely crack propagation. For each material, the crack propagation rate is higher under larger R ratio.
In Fig. 4(b), the crack propagation rate is correlated to the range of energy release rate, ΔG_I, which is defined by

$$\Delta G_I = G_{I\max} - G_{I\min} = H_I \left(K_{\max}^2 - K_{\min}^2 \right) = H_I \left[(1+R)/(1-R) \right] (\Delta K)^2 \tag{4}$$

It is interesting to see that the data of each material under $R=0.1$ and 0.5 tend to merge, and these is no big influence of R ratio. Still, there exists a slight difference among MD, TD and PPS.
For isotropic materials, the stress intensity factor divided by Young's modulus, $\Delta K/E$, is often used to correlate the crack propagation data for different materials. This parameter can be interpreted to represent the range of crack-tip radius as shown in Fig. 5 [8]. The crack-tip radius in orthotropic materials is [9]

$$\rho = (4/\pi) H_I G_I \tag{5}$$

so the range of crack-tip opening radius is given by

$$\Delta \rho = \rho_{\max} - \rho_{\min} = (4/\pi) H_I \Delta G_I \tag{6}$$

Fig. 6 shows the relation between crack propagation rate and a parameter representing crack-tip opening radius, $H_I \Delta G_I$. The data for MD, TD and PPS come closer, indicating this parameter plays a more role in crack propagation. Still in the figure, MD has a stronger resistance to crack propagation in comparison with TD and PPS.

Fatigue Crack Propagation under Mixed Loading of Mode I and II
Except for the cases of MD and TD, the direction of crack propagation is inclined to the loading axis and cracks propagate under mixed loading of mode I and II. The energy release rates for mode I and II were calculated by FEM for cracks propagating at the measured angle shown in Fig. 3. Fig. 7 shows the crack propagation rate as a function of the range of energy release rate for mode I, ΔG_I, for $R=0.1$. When compared at the same ΔG_I, the crack propagation rate is highest for PPS and gets slower with deceasing fiber angle. The data are bounded by the relation for MD and TD.
To check the contribution of mode II, the crack propagation rate is plotted in Fig. 8 against the range of the total energy release rate, ΔG_{total}, which is defined by

$$\Delta G_{total} = \Delta G_I + \Delta G_{II} \tag{7}$$

The data for 22.5°, 45°, 67.5° move only slightly toward right, because the amount of ΔG_{II} is small relative to ΔG_I.
Since crack propagation is mainly controlled by mode I loading and no equation is available for crack-tip opening for mixed mode loading, a parameter, $\Delta G_{total}/E$, is adapted as a rough estimate of the crack-tip opening radius for all cases including MD and TD, where E is Young's modulus given in Tab. 2. Fig. 9 shows the crack propagation rate correlated to $\Delta G_{total}/E$ for $R=0.1$ and 0.5. All data tend to merges into a single relation for $R=0.1$, while there is some scatter for $R=0.5$. This parameter would be useful to estimate the crack propagation law for various fiber orientation, though the physical meaning of this parameter needs to be explored in the future.
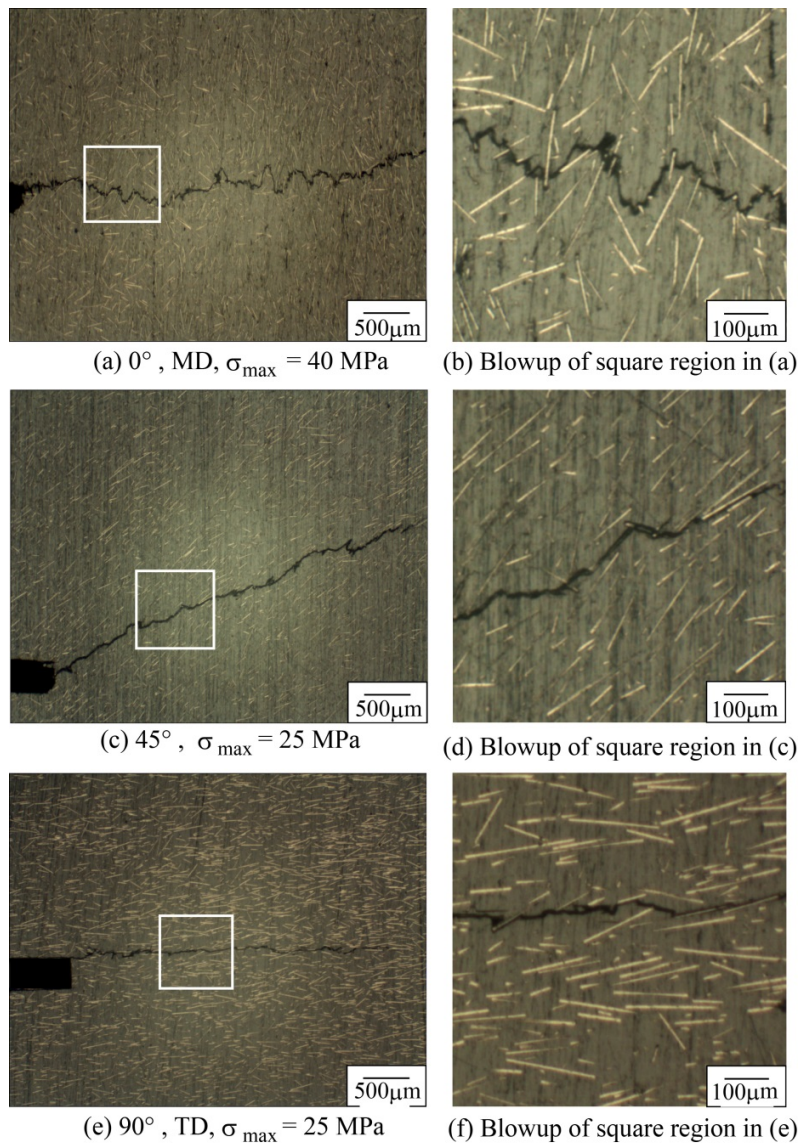
(a) 0° , MD, σ_{max} = 40 MPa (b) Blowup of square region in (a)

(c) 45° , σ_{max} = 25 MPa (d) Blowup of square region in (c)

(e) 90° , TD, σ_{max} = 25 MPa (f) Blowup of square region in (e)

Figure 2: Fatigue cracks in MD, 45°, TD specimens of IMP under R=0.1.
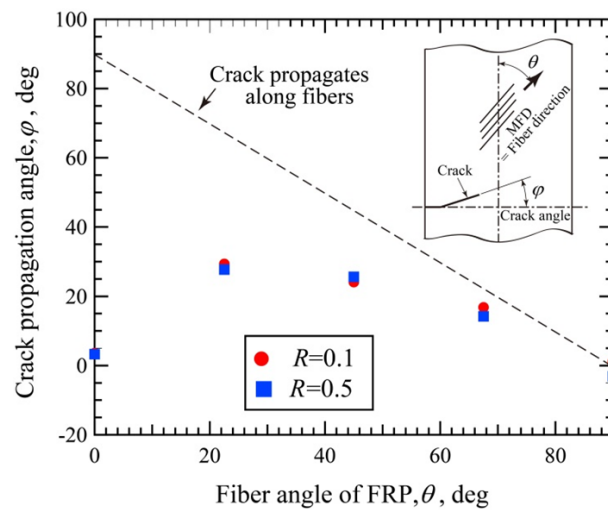
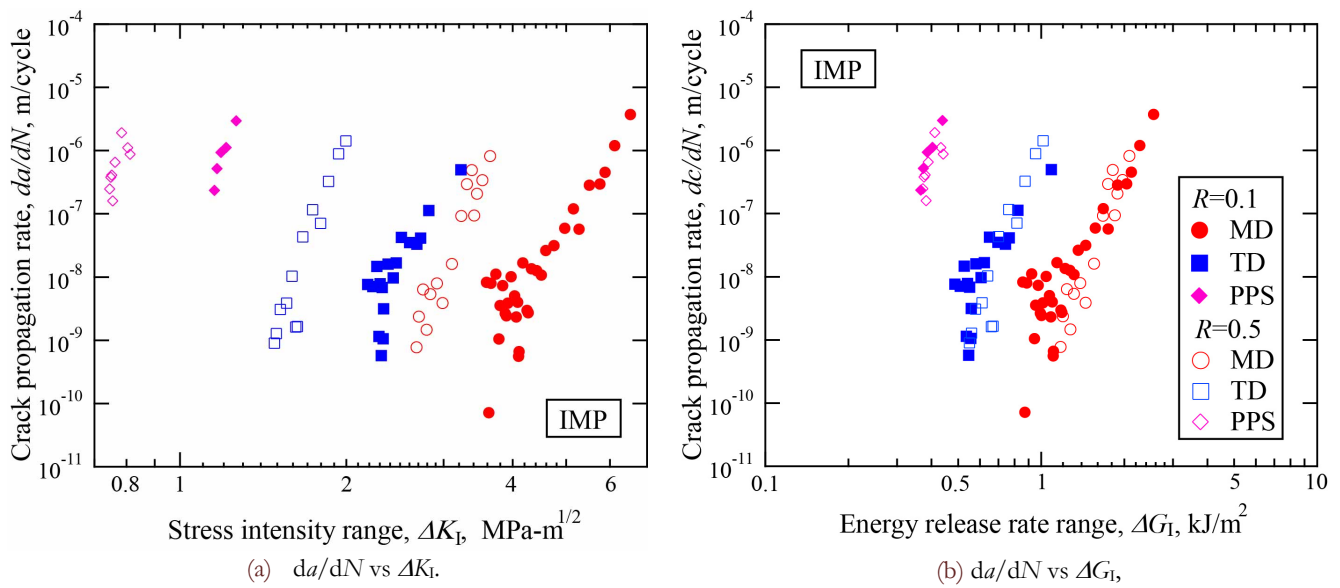Figure 3: Relation between crack propagation angle and fiber angle.

(a) da/dN vs ΔK_I.

(b) da/dN vs ΔG_I,

Figure 4: Crack propagation rate correlated to ranges of stress intensity factor and energy release rate.
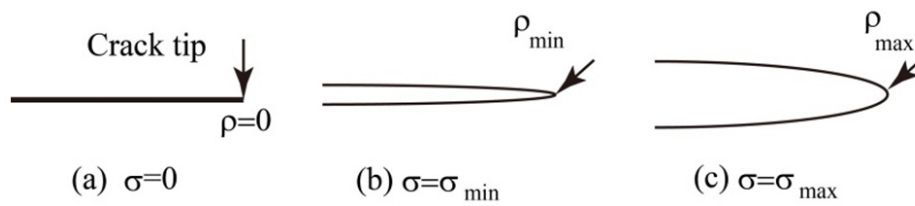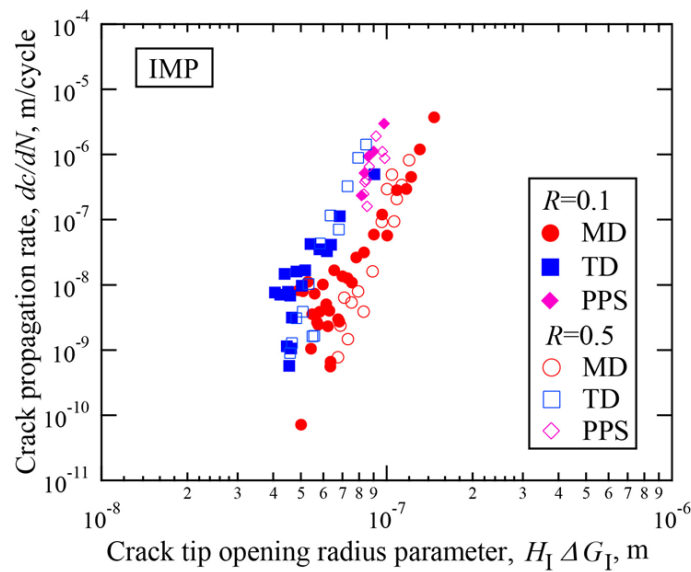

Figure 5: Change of crack-tip radius under loading.

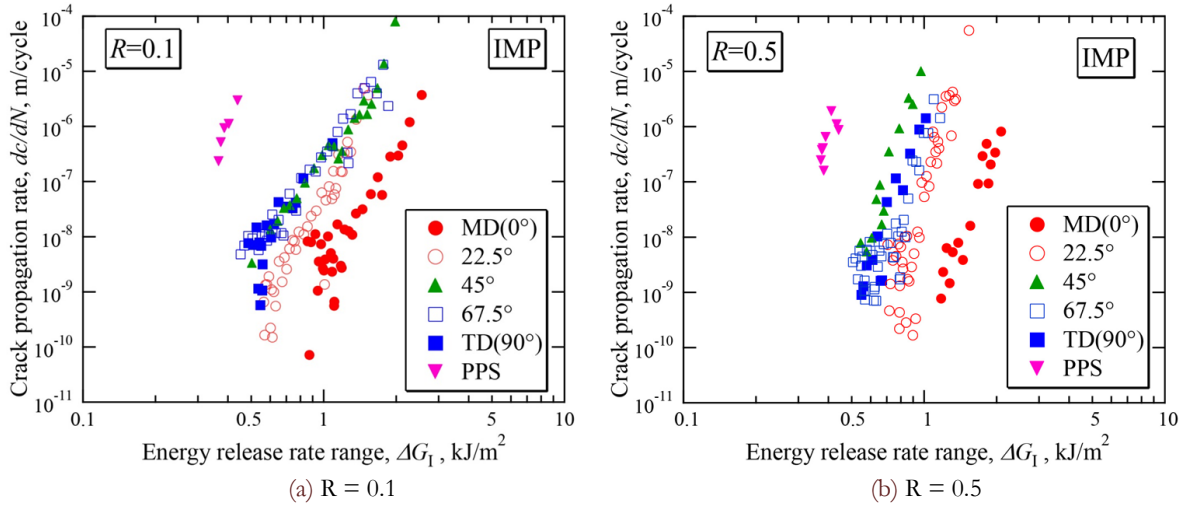Figure 6: Relation between crack propagation rate and crack-tip opening parameter.

(a) R = 0.1 (b) R = 0.5

Figure 7: Crack propagation rate correlated to the range of mode I energy release rate.

(a) R = 0.1 (b) R = 0.5
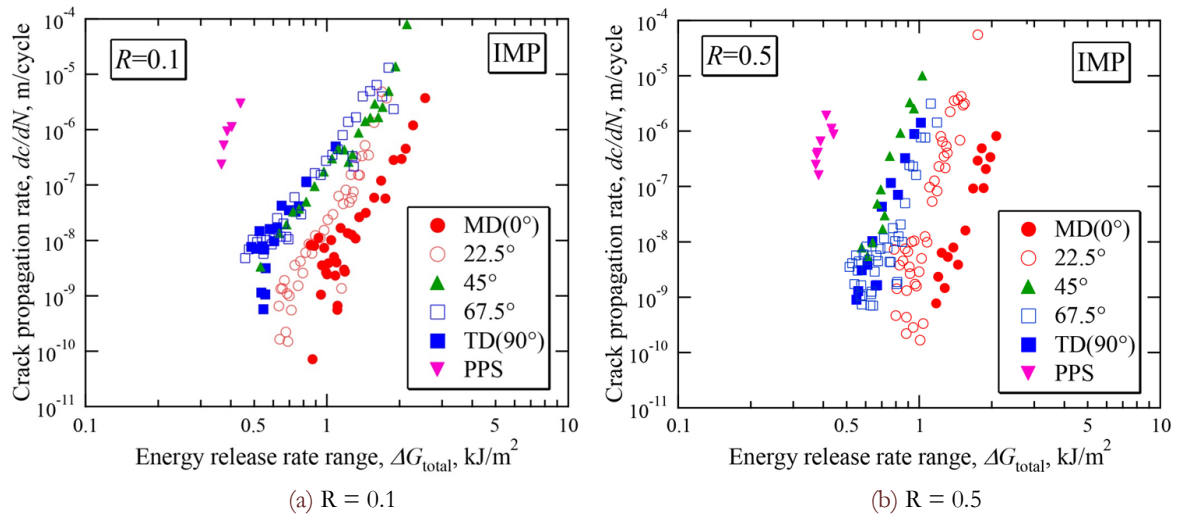
Figure 8: Crack propagation rate correlated to the range of total energy release rate.

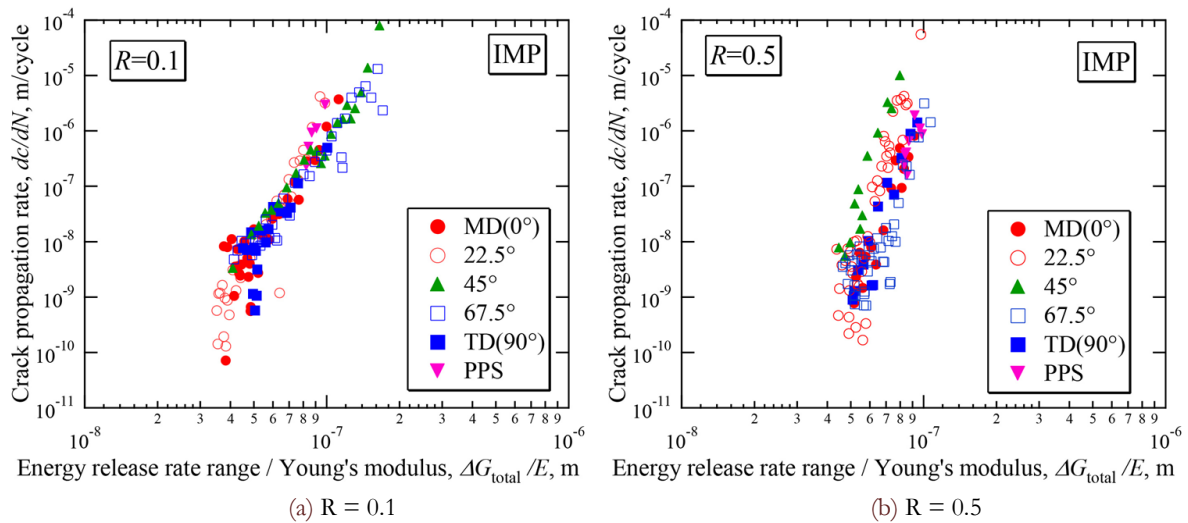

(a) R = 0.1 (b) R = 0.5

Figure 9: Relation between crack propagation rate and total energy release rate range divided by Young's modulus.

CONCLUSION

The influences of fiber orientation on the crack propagation behavior was studied with single edge-notched specimens which were cut from an injection-molded short fiber reinforced plastic plate at five fiber angles relative to the loading axis, i.e. $\theta = 0°$ (MD), 22.5°, 45°, 67.5°, 90° (TD), under the stress ratio R=0.1 and 0.5. Fracture mechanics parameter determined by FEM based on anisotropic elasticity were used to correlate the crack propagation rate. The obtained results are summarized as follows:

(1) Macroscopic crack propagation path was nearly perpendicular to the loading axis for the cases of MD and TD. For the other fiber angles, the crack path was inclined because the crack often propagated along fibers.

(2) For mode I crack propagation in MD and TD, the resistance to crack propagation is improved by fiber reinforcement, when the crack propagation rate is correlated the range of stress intensity factor. The crack propagation rate, da/dN, was slowest for MD and fastest for TD. For each material, the crack propagation rate is higher for larger R ratio. The effect of R ratio on da/dN diminished in the relation between da/dN and the range of energy release rate, ΔG_I.

(3) Difference among MD, TD and matrix resin becomes small when da/dN correlated to a parameter corresponding the crack-tip radius, $H_I \Delta G_I$, where H_I is compliance parameter.

(4) Fatigue cracks propagated under mixed loading of mode I and II for the fiber angles other than 0° and 90°. The data of crack propagation rate correlated to the range of total energy release rate, ΔG_{total} lie between the relations obtained for MD and TD.

(5) All data of crack propagation rates tend to merge a single relation when the rate is correlated to the range of total energy release rate divided by Young's modulus for various fiber angles and R ratios.

APPENDIX

FEM analyses were conducted using Marc Ver. 2005 to determine the energy release rate of mode I for MD and TD, and of mixed mode of I and II for the other fiber angles. The crack was assumed to propagate at the angle, φ, determined by experiments. Two-dimensional isoparametric eight-node rectangular elements were used under the condition of plane stress. The modified crack closure integral was adapted to determine the energy release rate. The orthotropic elastic constants used for FEM is given in Tab. 1. A load was applied to the edges of the central region of 20×50 mm² shown in Fig. 1 under constant displacement condition in the longitudinal direction. The calculated values of energy release rates were inserted in Eq. (1) and the correction factor, Y_I and Y_{II} were determined. For MD and TD, the stress intensity factor was determined by using Eq. (2) from the energy release rate.
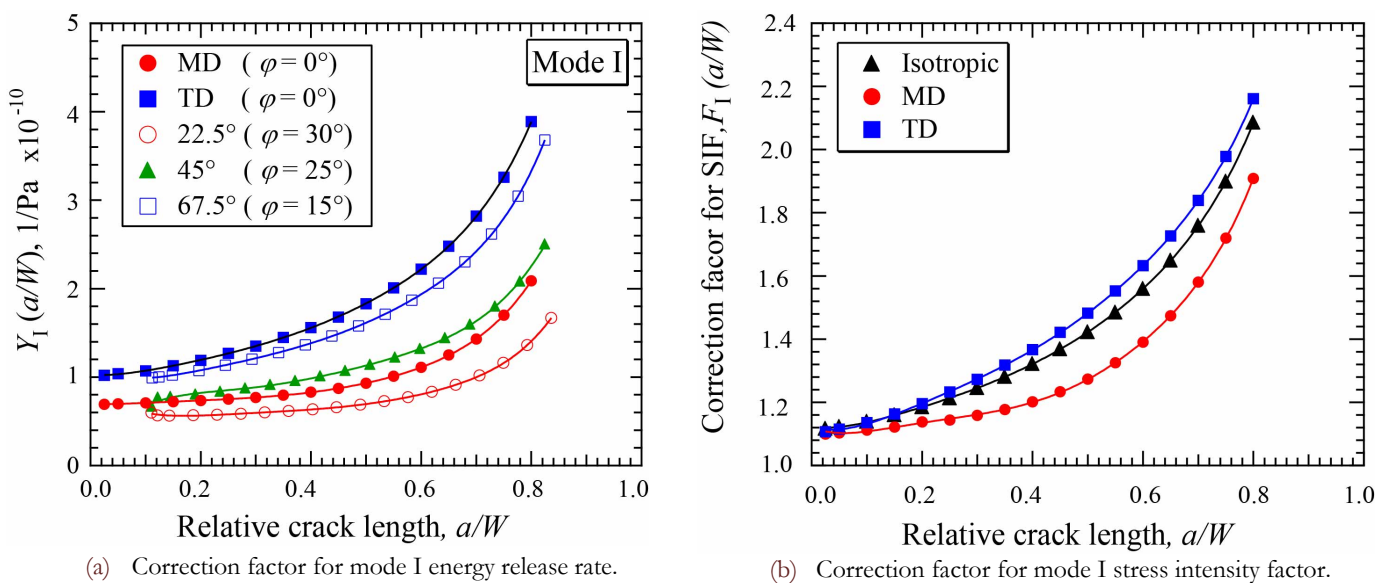

(a) Correction factor for mode I energy release rate.

(b) Correction factor for mode I stress intensity factor.

Figure 10: Correction factors of mode I energy release rate and stress intensity factor.

(a) Correction factor of mode II energy release rate.
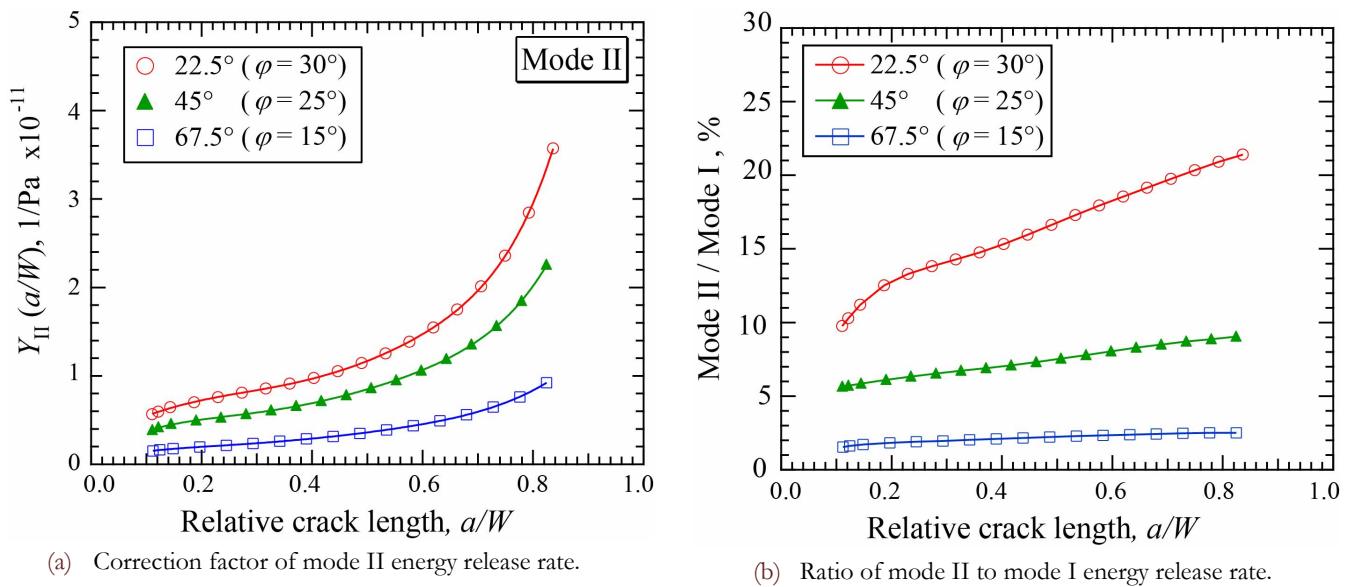
(b) Ratio of mode II to mode I energy release rate.

Figure 11: Correction factor of mode II energy release rate and ratio of mode II/mode energy release rate.

Fig. 10(a) shows the change of mode I energy release rate as a function of crack length. The correction factor increases with crack length. It is the largest for TD, and decreases with increasing crack propagation angle φ to 30°. For MD and TD, the correction factor F_I for an edge crack (φ =0) of the stress intensity factor is shown in Fig. 10(b), together with that for isotropic material. It is the largest for TD and smallest for MD, and that for isotropic material is in between.

Fig. 11(a) shows the change of mode II energy release rate for three fiber angles where the crack is inclined against the loading axis. The correction factor is the largest for 22.5° plate which has the largest crack angle φ =30°. In Fig. 11(b), the ratio of energy release rate of mode II to mode I is plotted against the crack length. It tends to increase with crack length, and is largest for the largest crack angle. The ratio is 20% at most.

The calculated data of energy release rate and stress intensity factor were used in the main text to determine the fracture mechanics parameters.

REFERENCES

[1] Mandel, J. F., Huang, D. D., McGarry, F. J., Fatigue of glass and carbon fiber reinforced engineering thermoplastics. Polymer Composites, 2 (1981) 137-144.

[2] Wyzgoski, M. G. , Novak, G. E., Fatigue fracture of nylon polymers, Part II Effect of glass-fiber reinforcement, Journal of Materials Science, 26 (1991) 6314-6324.

[3] Akiniwa, Y., Harada, S., Yagyu, Y., Nakano, M., Effect of fiber content and fiber orientation on fatigue strength of short-fiber reinforced plastics, Journal of Materials Science, Japan, 41 (1992) 1285-1291.

[4] Song, J. H., Lim, J.K., Kim, Y.J., Kim, H. G., Low cycle fatigue of PPS polymer injection welds – Fatigue crack behavior-. KSME International Journal, 17 (2003) 647-653.

[5] Tanaka, K., Kitano, T., Egami, N., Effect of fiber orientation on fatigue crack propagation in short-fiber reinforced plastics, Engineering Fracture Mechanics, 123 (2014) 44-58.

[6] Rybicki, E. F., Kanninen, M.F., A finite element calculation of stress intensity factors by a modified crack closure integral. Engineering Fracture Mechanics, 9 (1977) 931-938.

[7] Sih, G.C., Paris, P.C., Irwin, G. R., On crack in rectilinerly anisotropic bodies, International Journal of Fracture Mechanics, 1 (1965) 189-203.

[8] Pook, L. P., Frost, N. E., A fatigue crack growth theory, International Journal of Fracture Mechanics, 9 (1973) 53-61.

[9] Sih, G.C., Liebowitz, H., Mathematical theory of brittle fracture, in: H. Liebowitz (Ed.), Frature, Mathematical Fundamentals, Academic Press, New York, 2 (1968) 67-190.